Journal of Sound and Vibration (2002) **252**(3), 457–468
doi:10.1006/jsvi.2001.4000, available online at http://www.idealibrary.com on IDEAL®

AN OSCILLATION PHENOMENON OF REVERBERATION IN THE SHALLOW WATER WITH A THERMOCLINE

F. Li, G. Jin, R. Zhang and J. Liu

National Laboratory of Acoustics, Chinese Academy of Science, PO Box 2712, *Beijing* 100080, *China.*
E-mail: lfh@farad.ioa.ac.cn

AND

L. Guo

Department of Physics, Tsinghua University, Beijing 100084, *China*

(*Received* 23 *November* 2000, *and in final form* 4 *July* 2001)

An oscillation phenomenon of the reverberation intensity was observed in a recent shallow water reverberation experiment. This phenomenon cannot be explained by the widely used incoherent reverberation theory. In this paper, to explain the observed oscillation phenomenon, the modal interference of reverberation in the shallow water with a thermocline is discussed on the basis of the ray-mode theory. The theoretical analysis and numerical results show that modal interference can cause the regular oscillation phenomenon of the reverberation intensity, and the oscillation phenomenon of the reverberation intensity can be used to test different reverberation models.

1. INTRODUCTION

The predominant background interference of the active sonar in shallow water is often bottom reverberation. In the past few years, several reverberation models based on ray [1], PE [2], and normal mode [3, 4] theories have been developed. Those models mainly treat the propagation from the source to scatterers and from scatterers to the receiver.

The reverberation model based on normal mode, combined with ray-mode analogies, is one of the most practical models. The basic idea of this reverberation model was first introduced by Bucker and Morris, further developed by Zhang and Jin [3], and reviewed by Ellis [4]. Based on this model, good agreements have been obtained between the measured reverberation data and the incoherent reverberation calculations. In the past several decades, very less attention has been paid on the calculation of coherent reverberation in shallow water. At least the following two reasons make the discussion on the coherent reverberation theory extremely difficult: (1) The lack of information about the bottom scattering mechanics; (2) The range or frequency averaging of the measured data often makes the cross terms in the coherent reverberation calculation less important. Apparently, it is important to have a high-quality at-sea reverberation data base to test coherent reverberation numerical models and bottom scattering mechanism hypotheses.

An oscillation phenomenon of bottom reverberation loss, which cannot be explained by the incoherent theory of reverberation, was observed in the China–U.S. Yellow Sea Experiment in 1996. The details of this phenomenon are presented in section 2. To explain this phenomenon, the modal interference of the reverberation based on the coherent

0022-460X/02/$35.00

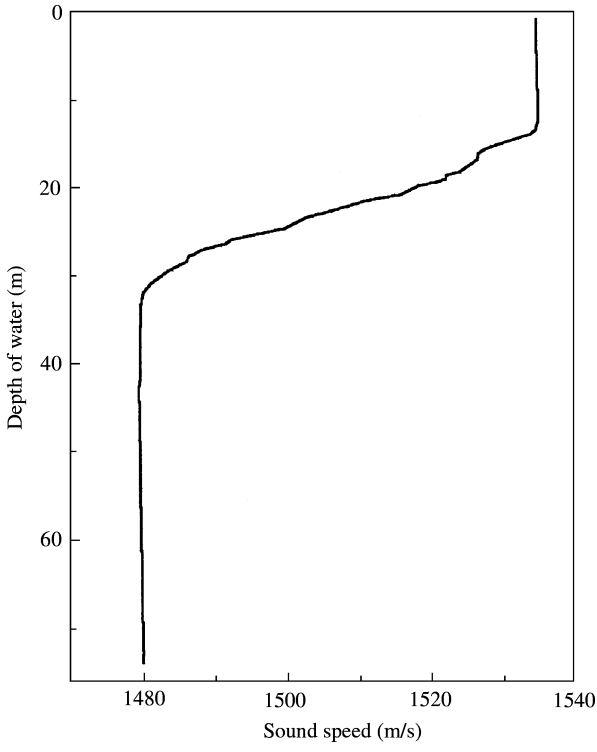

Figure 1. A sound speed profile during '96 Yellow Sea Experiment.

reverberation theory is discussed in section 3. In section 4, the comparisons of the numerical calculations and the measured data are presented, and some theoretical explanations are also given.

2. AN OSCILLATION PHENOMENON OF THE REVERBERATION

The joint China–U.S. Yellow Sea '96 Experiment was conducted over a 2-week period in August 1996 in the middle of the Yellow Sea. The summer conditions in the Yellow Sea produce an approximate three-layer sound-speed profile, with a near-linear thermocline connecting a warmer surface isovelocity layer to a cooler isovelocity bottom layer Figure 1. The explosives were detonated at depths of 7 and 50 m respectively. A vertical line array was used to receive the reverberation signals.

In the experiment, an oscillation phenomenon of reverberation loss was observed. In Figure 2 the reverberation losses versus time, which was received by the 32-element array are shown. The source was a charge of 1 kg TNT, which was detonated at a depth of 7 m. The hydrophone depths for figures (a), (b), (c), and (d) in Figure 2 were 6, 18, 20, and 50 m respectively. The central frequency of the measured data was 2000 Hz, and a 1/3oct-frequency averaging had been carried on the data. It can be seen from Figure 2 that only for the hydrophones at 18 and 20 m that were located within the thermocline, the received reverberation losses had a regular oscillation. This phenomenon has not been observed before and cannot be explained by the incoherent theory of reverberation [3, 4]. One possible hypothesis is that bubbles near the ocean surface may cause the oscillation

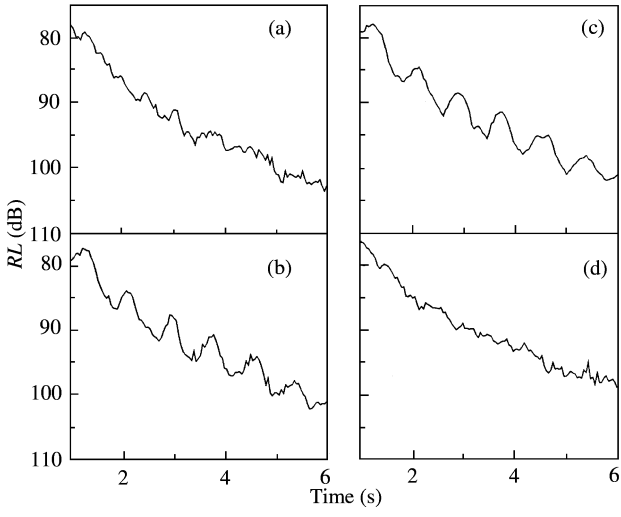

Figure 2. The reverberation loss versus time for the explosive source detonated at 7 m. The central frequency is 2000 Hz. The receiver depths are 6, 18, 20 and 50 for (a), (b), (c) and (d) respectively.

[5]. However, this hypothesis cannot explain as to why only for the receivers within the thermocline there is a regular oscillation of the reverberation intensity, and why the period of the reverberation loss oscillation on the time axis is 0·8 s. Alternative hypotheses are thus required in order to explain the data. In the next two sections, detailed discussions of this phenomenon and the coherent reverberation model will be presented.

3. THE COHERENT MODEL OF THE REVERBERATION

Figure 3 illustrates the reverberation generated by the bottom scattering. The reverberation pressure at the receiver $(z_r, 0)$ is often calculated by the summation of the sound pressures scattered from the bottom scattering elements over the area insonified by the incident pulse,

$$p(t) = \sum_i p_i, \tag{1}$$

where p_i is the sound pressure scattered from the ith bottom scattering element in a bottom circular ring with the radius of $ct/2$ and width of $c\tau/2$; τ is the signal duration.

By omitting the cross terms, the received reverberation intensity can be written as

$$I(t) = p(t)p^*(t)$$

$$= \sum_i |p_i|^2, \tag{2}$$

where the superscript star (*) denotes the complex conjugate.

The backscattering pressure p_i can be expressed as [3, 4]

$$p_i = \sum_m \sum_n \Theta_m(z_s, h)\, e^{i\mu_m r}\, \Theta_n(z_r, h)\, e^{i\mu_n r} D_i(\alpha_m, \alpha_n), \tag{3}$$

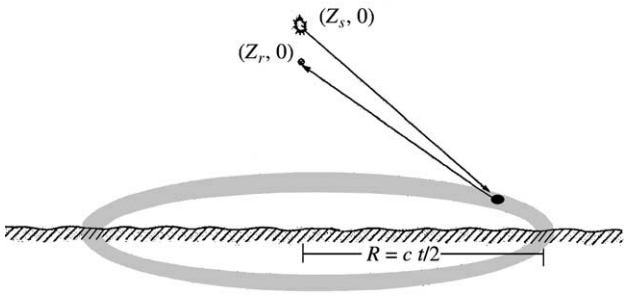

Figure 3. Schematic illustrating reverberation scattered from the bottom.

where

$$\Theta_m(z, h) = \left(\sqrt{\frac{8\pi}{r}} \frac{\sqrt{\mu_m}\, q_m(z)\, q_m(h)}{S_m} \sin\left[\varphi_m(z)\right] \mathrm{e}^{-\beta_m r} \right) \mathrm{e}^{\mathrm{i}[\varphi_m(h)]},$$

$$\varphi_m(z) = \int_{\zeta_m}^{z} \sqrt{k^2(y) - v_m^2}\, \mathrm{d}y + \theta_m,$$

$$q_m(z) = \left[0{\cdot}875 d^{2/3} + k^2(z) - \mu_m^2\right]^{-1/4}.$$

Combining equations (2) and (3) gives the reverberation intensity at the receiver scattered from the ith bottom scattering element,

$$\begin{aligned} I_i = p_i p_i^* &= \sum_m \sum_n |\Theta_m(z_s, z_b)|^2 \, |\Theta_n(z_r, z_b)|^2 \, |D_i(\alpha_m, \alpha_n)|^2 \\ &+ \sum_m \sum_{\substack{n \\ (n' \neq n)}} \sum_{n'} |\Theta_m(z_s, z_b)|^2 \, \Theta_n(z_r, z_b) \Theta_{n'}^*(z_r, z_b) \, D_i(\alpha_m, \alpha_n) \, D_i^*(\alpha_m, \alpha_{n'}) \, \mathrm{e}^{\mathrm{i}(\mu_n - \mu_{n'})r} \\ &+ \sum_n \sum_{\substack{m \\ (m' \neq m)}} \sum_{m'} |\Theta_n(z_r, z_b)|^2 \, \Theta_m(z_s, z_b) \, \Theta_{m'}^*(z_s, z_b) \, D_i(\alpha_m, \alpha_n) \, D_i^*(\alpha_m, \alpha_{n'}) \, \mathrm{e}^{\mathrm{i}(\mu_m - \mu_{m'})r} \\ &+ \sum_{\substack{m \\ (m' \neq m;}} \sum_{\substack{m' \\ n' \neq n)}} \sum_n \sum_{n'} \Theta_m(z_s, z_b) \, \Theta_{m'}^*(z_s, z_b) \, \Theta_n(z_r, z_b) \, \Theta_{n'}^*(z_r, z_b) \, D_i(\alpha_m, \alpha_n) \, D_i^*(\alpha_{m'}, \alpha_{n'}) \\ &\quad \times \mathrm{e}^{\mathrm{i}(\mu_m + \mu_n - \mu_{m'} - \mu_{n'})r}. \end{aligned} \tag{4}$$

The incoherent summation is obtained by assuming that the cross terms (the second, third, and fourth terms) in equation (4) can be neglected due to the average over frequency or space:

$$I_{inc} = E_0 \pi r c \sum_m \sum_n |\Theta_m(z_s, z_b)|^2 \, |\Theta_n(z_r, z_b)|^2 \, \sigma(\alpha_m, \alpha_n). \tag{5}$$

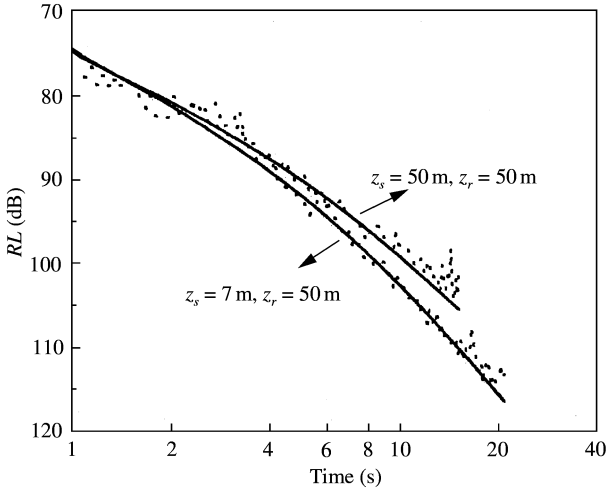

Figure 4. Comparisons of the experimental data and the incoherent model predictions for different source depths. The central frequency is 1000 Hz.

For the Lambert model, one has $\sigma(\alpha_m, \alpha_n) = \mu \sin\alpha_m \sin\alpha_n$, where α_m and α_n are, respectively, incident and scattering grazing angles.

The reverberation loss is defined as

$$RL_{inc} = 10\log_{10}\frac{E_0}{I_{inc}}$$

$$= -10\log_{10}\left[\pi rc\sum_m\sum_n |\Theta_m(z_s, z_b)|^2\,|\Theta_n(z_r, z_b)|^2\,\sigma(\alpha_m, \alpha_n)\right]. \tag{6}$$

In many cases, the cross terms (the second, third, and fourth terms) in equation (4) can indeed be neglected due to averages over both frequency and space, and equation (6) provides a good explanation for many experimental data. The experimental reverberation losses for several frequencies and source depths in the Yellow Sea Experiment are compared in Figures 4 and 5 with the numerical calculations from equation (6). The receiver depth in Figures 4 and 5 is 50 m which is outside the thermocline. In those figures, the solid lines are calculated by equation (6), and the dotted lines indicate the experimental data. The bottom parameters used in equations (1) and (4) are from reference [6], and the Lambert scattering model is used. It can be seen from the figures that the numerical results and experimental data are in good agreement.

However, the incoherent model cannot predict the oscillation phenomenon shown in Figure 2 when the receiver is within the thermocline. Numerical calculations show that in shallow water with a thermocline, when the source is above or below the thermocline, the third and fourth terms in equation (4) can be neglected after an averaging over frequency due to the interference of a large number of cross terms with factors $e^{i(\mu_m - \mu_{m'})r}$. If the receiver is not within the thermocline, the second term in equation (4) can also be neglected due to the same reason. If the receiver is within the thermocline, only a few scattering normal modes have significance effects on the reverberation, and the modal interference cannot be neglected, which will be discussed in the following.

Figure 6 shows the amplitudes, cycle-distances, and grazing angles of different normal modes, where the frequency is 2000 Hz, and z in $|\Theta_m(z, h)|^2$ is 19 m, which is within the

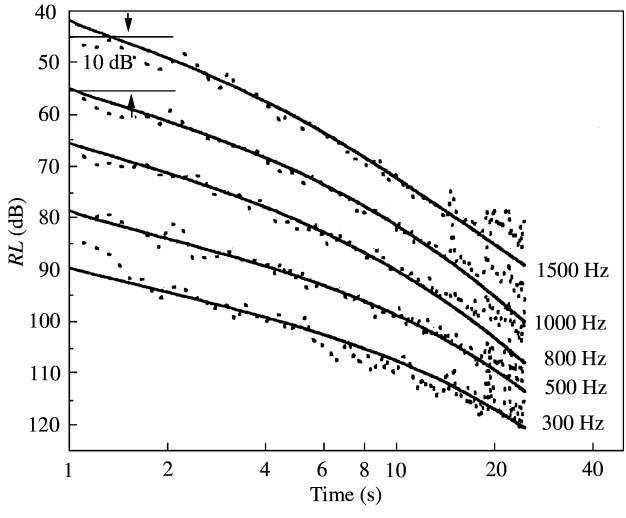

Figure 5. Comparisons of the experimental data and the incoherent model predictions for different frequencies. The depths of the source and receiver are 7 and 50 m respectively.

thermocline. In Figure 6(a) it is shown that when the receiver is within the thermocline, only a few modes have large amplitudes (between the two dashed lines in Figure 6). These modes are often called effective normal modes, and the grazing angles of those normal modes are called effective grazing angles. It can be seen from Figure 6(b) that when the receiver is within the thermocline, the effective grazing angles are within a small range of angle, which is about 12 to 15°. In general, the scattering directivity $D_i(\alpha_m, \alpha_n)$ is complicated and difficult to measure. However, it is reasonable to assume that for each scattering element, $D_i(\alpha_m, \alpha_n)$ is almost a constant in such a small range of effective scattering grazing angle, that is

$$D_i(\alpha_m, \alpha_n) \approx D_i(\alpha_m, \alpha_c), \tag{7}$$

where α_c is the median of effective scattering grazing angle.

On combining equations (4) and (7), the coherent reverberation intensity [7] and the coherent reverberation loss which include the effect of the modal interference can be written as

$$I_{coh} = E_0 \pi r c \left[\begin{array}{l} \sum_m \sum_n |\Theta_m(z_s, z_b)|^2 \, |\Theta_n(z_r, z_b)|^2 \, \sigma(\alpha_m, \alpha_n) \\ + \sum_m \sum_{(n' \neq n)} \sum_{n'} |\Theta_m(z_s, z_b)|^2 \, \Theta_n(z_r, z_b) \, \Theta_{n'}^*(z_r, z_b) \, \sigma(\alpha_m, \alpha_c) \, \mathrm{e}^{\mathrm{i}(\mu_n - \mu_{n'})r} \end{array} \right], \tag{8}$$

$$RL_{coh} = 10 \log_{10} \frac{E_0}{I_{coh}}$$

$$= -10 \log_{10} \left\{ \pi r c \left[\begin{array}{l} \sum_m \sum_n |\Theta_m(z_s, z_b)|^2 \, |\Theta_n(z_r, z_b)|^2 \, \sigma(\alpha_m, \alpha_n) \\ + \sum_m \sum_{(n' \neq n)} \sum_{n'} |\Theta_m(z_s, z_b)|^2 \, \Theta_n(z_r, z_b) \, \Theta_{n'}^*(z_r, z_b) \, \sigma(\alpha_m, \alpha_c) \, \mathrm{e}^{\mathrm{i}(\mu_n - \mu_{n'})r} \end{array} \right] \right\}. \tag{9}$$

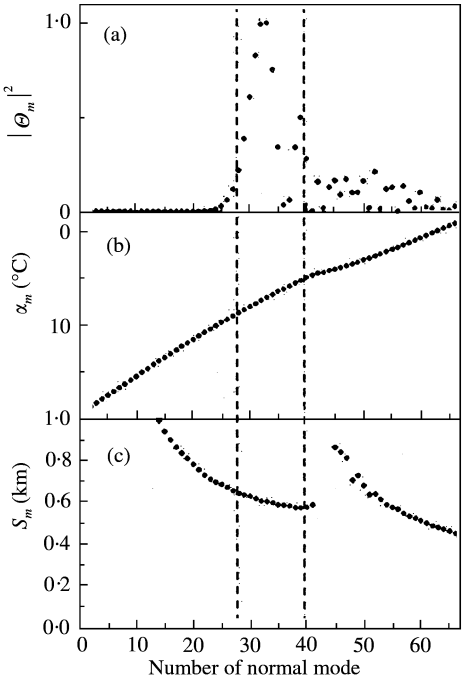

Figure 6. The comparison of the amplitudes, the cycle-distances, and the grazing angles of different normal modes, where the frequency is 2000 Hz, and z in $|\Theta_m(z, h)|^2$ is 19 m.

4. NUMERICAL RESULTS AND COMPARISONS WITH DATA

In Figures 7 and 8, the comparisons of the coherent reverberation loss, incoherent reverberation loss and the measured data are given. In the figures, the solid lines indicate the experimental reverberation data, the dashed lines indicate the incoherent reverberation losses calculated from equation (6), and the dotted lines indicate the coherent reverberation losses calculated from equation (9). The bottom parameters are taken from reference [6]. The receiver depths for figures (a) and (b) in Figures 7 and 8 are 18 and 20 m respectively. In Figures 7 and 8, the source depths are, respectively, 50 and 7 m, and the, frequencies are, respectively, 1000 and 2000 Hz. It can be seen from the figures that the numerical results from the coherent reverberation model can predict the oscillation phenomenon and are in better agreement with the measured data.

To explain the oscillation phenomenon theoretically, further discussions of the modal interference are presented in the following. Based on the BDRM theory [8], one has

$$\begin{aligned} \mu_m &\approx \mu_{m-1} - \frac{2\pi}{S_{m-1}} \\ &\sim \mu_{m-2} - \left(\frac{2\pi}{S_{m-1}} + \frac{2\pi}{S_{m-2}}\right), \\ &\sim \mu_n - 2\pi \sum_{i=n}^{m-1} \frac{1}{S_i}, \end{aligned} \tag{10}$$

where S_i is the cycle-distance of ith normal mode.

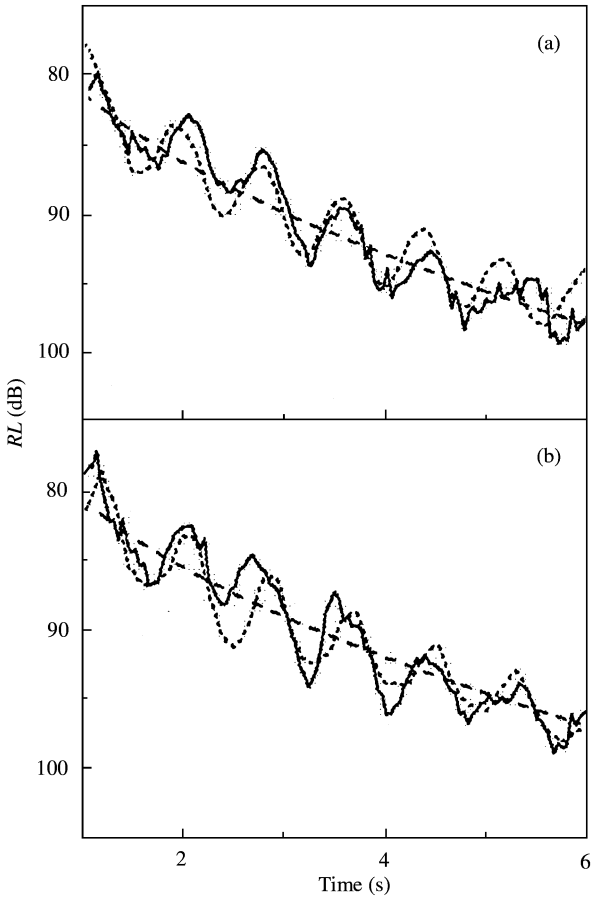

Figure 7. The comparisons of the calculated coherent reverberation losses (dotted line), incoherent (dashed line) reverberation losses and the measured data (solid line). The center frequency is 1000 Hz, the source depth is 50 m, and the receiver depths are, respectively, 18 and 20 m for (a) and (b).

From Figure 6(c), when the receiver is within the thermocline, the cycle-distances of the effective scattering normal modes can be approximated as a constant,

$$S_i \approx S_c, \tag{11}$$

On substituting equations (10) and (11) into equation (9), one obtains

$$RL_{coh} = -10\log_{10} \times \left\{ \pi r c \left[\begin{array}{l} \displaystyle\sum_m \sum_n |\Theta_m(z_s, z_b)|^2 |\Theta_n(z_r, z_b)|^2 \sigma(\alpha_m, \alpha_n) \\ \displaystyle + \sum_m \sum_{\substack{n \\ (n' \neq n)}} \sum_{n'} |\Theta_m(z_s, z_b)|^2 \Theta_n(z_r, z_b) \Theta_{n'}^*(z_r, z_b) \sigma(\alpha_m, \alpha_c) \, \mathrm{e}^{\mathrm{i}(2\pi(n-n')/S_c)r} \end{array} \right] \right\}. \tag{12}$$

From equation (12), it can be seen that the second term has a space period of $R = S_c$, which is $T = 2R/c = 2S_c/c$ on the time axis. The cycle-distances of the effective scattering

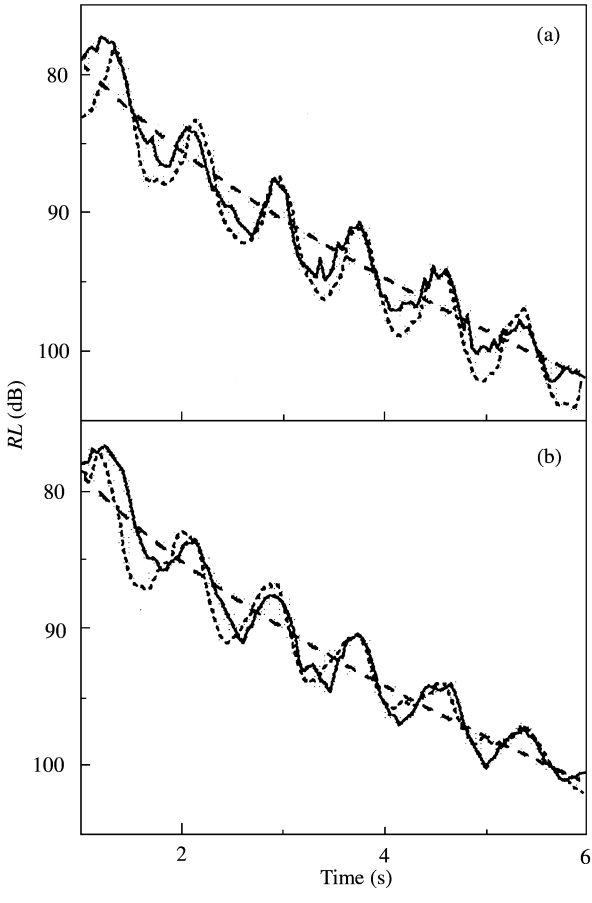

Figure 8. The comparisons of the calculated coherent reverberation losses (dotted line), incoherent (dashed line) reverberation losses and the measured data (solid line). The center frequency is 2000 Hz. The source depth is 7 m, and the receiver depths are, respectively, 18 and 20 m for (a) and (b).

normal modes are about 600 m from Figure 6(c). Hence, the period of the reverberation loss oscillation on the time axis is about $T = 2 \times 600/1500 = 0{\cdot}8$ s, which agrees with the experimental data in Figures 7 and 8.

It should also be pointed out that the oscillation phenomenon of the reverberation in Figures 7 and 8 is due to the interference of the normal modes. The bottom reverberation is the sound field scattered from the bottom scattering elements. In Figure 9, the sound speed profile and rays which emanate from the bottom within an aperture of 15° (steeper rays have large attenuations or very small eigenfunctions at the receiver within the thermocline) are shown. It can be seen from the figure that in the thermocline, there is something like a convergence zone and shadow zone in deep water. The convergence-zone range is about 600 m, which agrees with the period of the reverberation loss oscillation. From the viewpoint of normal modes, this convergence zone and shadow zone are due to normal mode interference. Hence, when the source is close to the bottom, and the receiver is within the thermocline, the transmission loss will also exhibit a similar oscillation phenomenon. Figures 10 and 11 give the numerical results of the transmission loss calculated by the BDRM [8] theory. In the figures, the source depth is 75 m, and the receiver depths for figures (a) and (b) in Figures 10 and 11 are 18 and 20 m respectively. The central

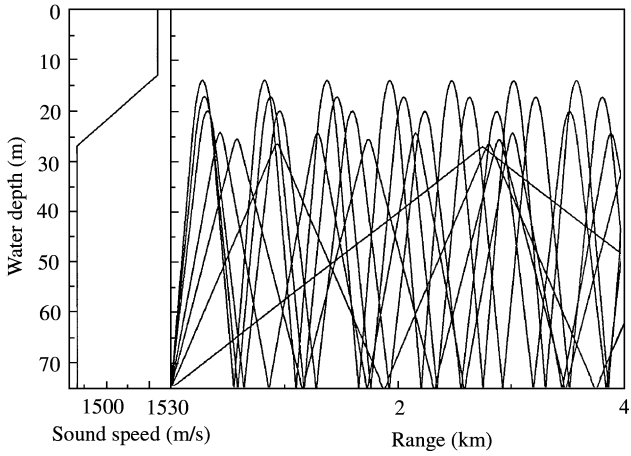

Figure 9. Sound speed profile and rays that emanate from the bottom within an aperture of 15°.

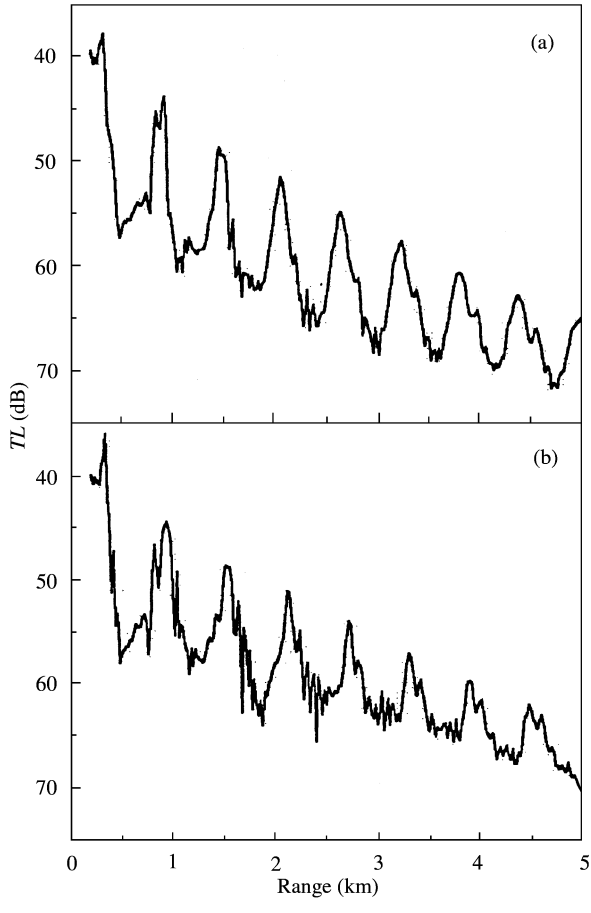

Figure 10. The transmission losses predicted by BDRM theory. The frequency is 1 kHz. The source depth is 75 m. The receiver depths are, respectively, 18 and 20 m for (a) and (b).

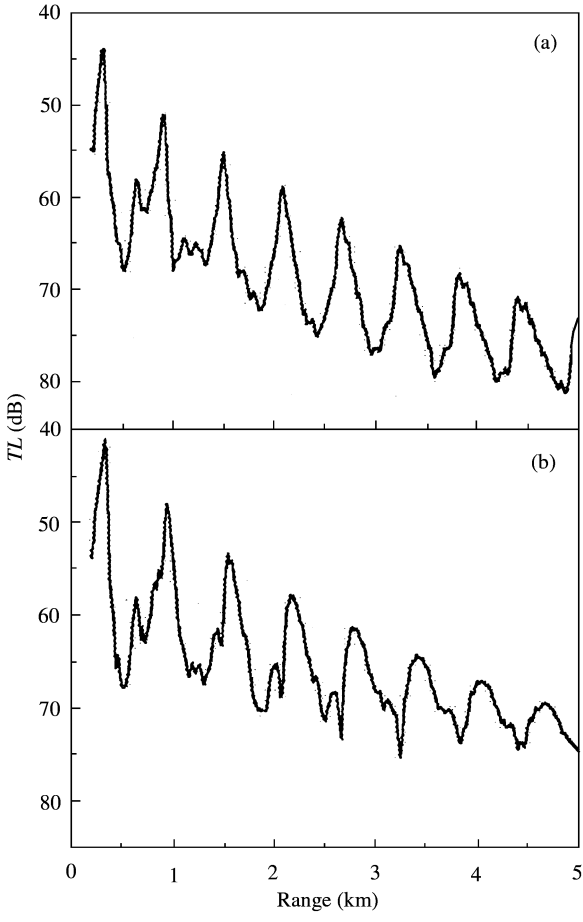

Figure 11. The transmission losses predicted by BDRM theory. The frequency is 2 kHz. The source depth is 75 m. The receiver depths are, respectively, 18 and 20 m for (a) and (b).

frequencies in Figures 7 and 8 are 1 and 2 kHz, respectively, and a 1/3oct-frequency averaging has been carried out on the results. The sound speed profile and the bottom parameters are the same as those in the above section. It can be seen from the figures that the transmission losses also exhibit the oscillation phenomenon at a period of about 600 m, which agrees with that of the reverberation.

5. SUMMARY

In this paper, an oscillation phenomenon observed in the China–U.S. Yellow Sea Experiment is described. The modal interference of the reverberation based on the coherent ray-mode reverberation theory is discussed, and is used to explain the observed oscillation phenomenon of shallow water reverberation. The results show that in shallow water with a thermocline, when the receiver is within the thermocline, there occurs an oscillation phenomenon of the reverberation intensity, which is due to the interference of the normal modes. The numerical results also indicate that there may exist an oscillation phenomenon of the transmission loss when the receiver is within the thermocline and when the source is

near the bottom. The oscillation phenomenon of the reverberation intensity shown in this paper can also be used to test the different reverberation models.

ACKNOWLEDGMENTS

This work was funded by the Natural Science Foundation of China and ONR.

REFERENCES

1. C. WU 1979 *Acta Acustica* **4**, 114–119. Calculation of shallow water reverberation intensity based on ray theory.
2. M. D. COLLINS, G. J. ORRIS and W. A. KUPERMAN 1993 in *Ocean Reverberation* (D. D. Ellis, J. R. Preston and H. G. Urban, editors), 119–224. Netherlands: Kluwer Academic Publishers. Reverberation modeling with two-way parabolic equation.
3. R. ZHANG and G. JIN 1987 *Journal of Sound and Vibration* **119**, 215–223. Normal-mode theory of average reverberation intensity in shallow water.
4. D. D. ELLIS 1995 *Journal of the Acoustial Society of America* **97**, 2804–2814. A shallow-water normal-mode reverberation model.
5. F. HENYEY 1991 *Journal of the Acoustial Society of America* **90**, 399–405. Acoustic scattering from ocean microbubble plumes in the 100 Hz to 2 kHz region.
6. F. LI and R. ZHANG 2000 *Acta Acustica* **25**, 297–302. The bottom speed and attenuation inverted by waveform and transmission loss.
7. F. LI, R. ZHANG and G. JIN 1999 in *IWAET*'99 (X. Xu, editor), 70–77. Harbin Engineering University Press. The coherent theory and an oscillation phenomenon of the reverberation in shallow water.
8. R. ZHANG and F. LI 1999 *Science in China* **42**, 739–749. Beam-displacement ray-mode theory of sound propagation in shallow water.

APPENDIX A: NOMENCLATURE

ω	angular frequency
$c(z)$	sound speed
$k(z)$	wavenumber, $k(z) = \omega/c(z)$
α_m	the grazing angle of the mth normal mode, which is determined by $k(h)\cos\alpha_m = \mu_m$
$D_i(\alpha_m, \alpha_n)$	the scattering directivity of the ith bottom scattering element
v_m	the complex eigenvalue of normal mode, i.e., $v_m = \mu_m + \mathrm{i}\beta_m$
S_m	the cycle-distance of the eigenray
θ_m	a factor determined by the surface reflection phase
d	the slope of $k^2(z)$, $d = \mathrm{d}k^2(z)/\mathrm{d}z$
E_0	the energy flux density of the transmitting signal at unit distance
$\langle\ \rangle$	the statistical average over the bottom scattering area
N	the scattering number per unit area.
$\sigma(\alpha_m, \alpha_n)$	the bottom scattering coefficient, $\sigma(\alpha_m, \alpha_n) = N\langle D_i(\alpha_m, \alpha_n)\rangle$